Sakarya Üniversitesi Fen Bilimleri Dergisi
Sakarya University Journal of Science

e-ISSN : 2147-835X
Publisher : Sakarya University

Vol. 29, No. 3, 272-284, 2025
DOI: https://doi.org/10.16984/saufenbilder.1576155

Research Article

The Mechanical Properties of 6061-T6 Aluminum Alloy Joints Joined by MIG Welding Method (TPS/i) Using Different Shielding Gas Flow Rates

Erman Ferik[1*], Sedat Dağlaraştı[2], Faruk Varol[3]

[1] Marmara University, Faculty of Technology, Department of Metallurgical and Materials Engineering, İstanbul, Türkiye, erman.ferik@marmara.edu.tr, ror.org/02kswqa67
[2] Türkiye Rail System Vehicles Inc., Sakarya, Türkiye, sedatdaglarasti@gmail.com
[3] Sakarya University of Applied Sciences, Vocational School of Information Technologies, Department of Machinery, Sakarya, Türkiye, fvarol@subu.edu.tr, ror.org/01shwhq58
[*]Corresponding Author

ARTICLE INFO

Keywords:
6061-T6
Aluminum
MIG Welding
Tensile strength

Article History:
Received: 30.10.2024
Revised: 05.03.2025
Accepted: 08.04.2025
Online Available: 10.06.2025

ABSTRACT

In this study, aluminum 6061-T6 alloy sheets with a thickness of 3 millimeters were welded using the TPS/i MIG welding process. Welded samples were joined in the shape of butt joints. Argon was used as the welding shield gas, and the welded joint procedures were carried out at various shielding gas flow rates. Tensile strength and hardness values of the welded 6061-T6 aluminum alloy sheets were determined, and their microstructure and macrostructure were investigated using an optical microscope. The weldability of 6061-T6 aluminum sheets was investigated using the MIG welding process (TPS/i), and the impact of various shielding gas flow rates on mechanical parameters, macrostructures, and microstructures was studied.

1. Introduction

1.1. Aluminum's main features

Aluminum is a widely used and versatile metal that plays a crucial role in various industries, including aerospace and construction. Its low weight, corrosion resistance, and excellent thermal conductivity make it an ideal material for transportation across air, land, and sea, particularly in applications demanding a high strength-to-weight ratio.

The mechanical properties and strength of pure aluminum have been enhanced by incorporating alloying elements such as silicon, magnesium, and copper. As a result of advancements in aluminum alloy production, aluminum can now be employed in demanding environments, including aerospace and marine applications [1-10].

The 6061-T6 aluminum alloy examined in this study has a high concentration of magnesium and silicon. It is distinguished by its superior strength, excellent corrosion resistance, ease of fabrication, and good weldability. The T6 hardening process is a heat treatment that enhances the mechanical properties of aluminum alloys, particularly yield strength, tensile strength, and hardness in 6061 [11-15].

1.2. Welding procedure, MIG welding method and TPS/i

Welding is a widely utilized manufacturing technique across various industries, such as aerospace, automotive, and energy, for joining metals and thermoplastics. The resulting connection is known as a welded joint [16-18].

In the MIG/MAG welding process, the heat produced by an electric arc between a consumable metal electrode and the workpiece

Cite as: E. Ferik, S. Dağlaraştı, F. Varol, "The mechanical properties of 6061-T6 aluminum alloy joints joined by MIG welding method (TPS/i) using different shielding gas flow rates," Sakarya University Journal of Science, vol. 29, no. 3, pp. 272-284, 2025. https://doi.org/10.16984/saufenbilder.1576155

generates a weld pool, which facilitates the fusion of the electrode and workpiece to create a welded joint.

In the MIG welding process, an inert gas such as argon or helium shields the arc and weld pool, whereas in the MAG welding method, an active gas like carbon dioxide protects them from environmental influences and contaminants. The MIG/MAG welding technique is widely used for welding low-alloy and unalloyed steels, high-alloy steels, stainless steels, and aluminum components [19-24].

Welding aluminum presents several challenges due to its inherent properties. Aluminum exhibits a strong affinity for oxygen, leading to the formation of an Al_2O_3 oxide layer on its surface. This oxide layer has a significantly higher melting point (2050°C) than aluminum itself, which melts at a much lower temperature. Consequently, it is essential to take preventive measures to inhibit oxide formation before welding. Moreover, aluminum and its alloys possess a high thermal conductivity, necessitating a greater heat input compared to steel to achieve the required heat concentration at the welding site.

Due to aluminum’s substantial thermal expansion, welding processes often result in considerable distortions and internal stresses. Failure to implement appropriate precautions can lead to stress-induced cracks. Hot cracking is particularly prevalent in alloys with a broad solidification range, such as AlMn, AlSi, AlCu, and AlMg, and typically occurs along the solidus line or within the solidification zone. The most common challenges encountered in aluminum welding include oxidation, porosity, contamination, and hot cracking [25].

TPS/i (TransPuls Synergic/intelligent) is a pulsed-arc MIG/MAG welding system. Synergic refers to the machine's real-time adjustment of welding parameters such as voltage, current, wire feed speed, and other settings. This functionality means that if you modify one parameter, the others are automatically modified to provide the optimum overall welding performance. This can help welders, especially those without prior welding expertise, produce consistent, high-quality welds with minimal human intervention [26].

Shielding gas in MIG welding serves to protect the weld pool from contamination while also affecting various welding characteristics. These include arc stability, metal transfer type, penetration, wetting, weld seam geometry, heat input, welding speed, weld metal composition, smoke production, and mechanical properties. Increasing the shielding gas flow rate improves penetration and bead width but has minimal impact on deposition rate and bead size. Conversely, reducing the flow rate decreases penetration and bead width without affecting deposition rate or bead size. The optimal shielding gas flow rate depends on several factors, such as welding current, joint geometry, gas type, nozzle size, welding position, metal transfer mode (short arc, long arc, or spray arc), workpiece material (e.g., aluminum, stainless steel, or carbon steel), material thickness, joint preparation, and cost [27, 28].

During welding, the electrode, weld bead, and weld pool are subjected to various forces, including electromagnetic force, plasma shear voltage, arc pressure, surface tension, and gravity. The droplet detaches from the electrode tip and is transferred to the weld pool, where it solidifies to form the weld bead. This process is governed by the balance of these forces and is significantly influenced by welding parameters, particularly shielding gas. Shielding gases play a crucial role in altering these forces, thereby affecting metal transfer mode, weld penetration shape, weld bead size and form, and other welding characteristics. Therefore, selecting the appropriate shielding gas is essential for optimizing welding performance and minimizing the risk of fusion defects that could compromise structural integrity [29, 30].

In addition to optimizing parameters such as welding current and torch angle, the proper selection and use of shielding gases play a crucial role in determining weld quality. The shielding gas flow rate significantly impacts the final weld outcome; an insufficient flow rate fails to adequately protect the weld area, leading to contamination by atmospheric gases. This issue is typically mitigated by increasing the shielding gas flow rate. However, an excessively high flow rate can create turbulence, drawing in atmospheric gases and compromising weld integrity. Due to the intense heat within the arc column, atmospheric gases become dissociated, absorbed, and dispersed into the weld pool. If buoyancy forces are insufficient to allow these gases to escape from the molten metal, porosity develops, trapping gas bubbles and resulting in voids within the solidified weld [31-36].

Argon is the most widely used gas in the industry due to its availability and lower cost compared to other inert gases. Since it is denser than air, it is primarily suitable for shielding welds in flat positions and deep groove joints, requiring a lower flow rate. Pure argon is commonly used for welding aluminum and other nonferrous metals. It offers excellent arc stability, effective cleaning action, and strong arc initiation properties. Additionally, it efficiently generates plasma, ensuring a steady and smooth-burning arc while exhibiting excellent electrical conductivity [37].

This study examines the TPS/i welding of 6061-T6 aluminum sheets using aluminum-based welding wire. The results indicate that while the welded samples exhibited lower strength than the base material, they still met the required acceptability standards. This article primarily explores the microstructure, strength characteristics, and welding processes of aluminum sheet joints produced using the TPS/i welding technique.

2. Material and Method

This study utilized 6061-T6 aluminum alloy sheets, commonly used in railway car construction. The chemical composition of these aluminum alloy sheets is presented in Table 1.

Table 1. Chemical composition of 6061-T6 aluminum alloy sheets ((Elements (wt%))

Fe	Si	Mn	Cr	Ti
0.451	0.653	0.123	0.144	0.0466
Cu	**Mg**	**Zn**	**Al**	
0.242	0.844	0.0612	97.5	

The mechanical characteristics of 6061-T6 sheets are presented in Table 2.

Table 2. Mechanical properties of 6061-T6 aluminum alloy sheets

Yield Strength (N/mm^2)	Tensile Strength (N/mm^2)	Elongation (%)
260	285	12

The 6061-T6 aluminum alloy sheets were cut to dimensions of 150×300×3 mm. The dimensions of the samples are illustrated in Figure 1.

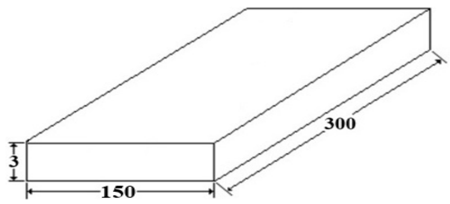

Figure 1. Dimensions of cut parts (mm)

Figure 2 shows the measurements of the welded samples.

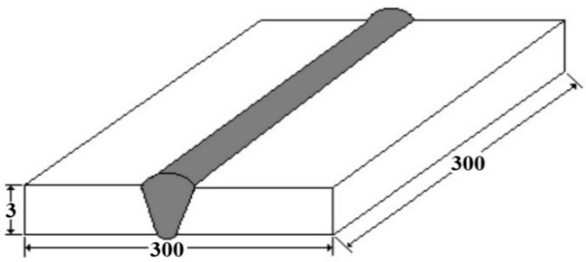

Figure 2. Dimensions of welded parts (mm)

The samples were chemically pre-cleaned with isopropyl alcohol before welding. Al 5356 welding filler metal, with a thickness of 1.2 mm, was used for the welding process. The welding was conducted in the PA position using a butt joint (BW) configuration. High-quality argon served as the shielding gas, with three different flow rates selected: 5 l/min, 12 l/min, and 20 l/min. The chemical composition of the welding filler wire is presented in Table 3.

Table 3. Chemical composition of Al 5356 welding filler wire ((Elements (wt%))

Fe	Si	Mn	Cr	Ti
0.40	0.25	0.10	0.10	0.10
Cu	**Mg**	**Zn**	**Al**	
0.10	4.75	0.10	94.1	

2.1. Welding procedure

The aluminum sheets were welded using a MIG welding machine (Fronius TPS 400i), where the shielding gas flow rates were varied while maintaining all other parameters constant. MIG welding (TPS/i) was carried out at three different shielding gas flow rates: 5 l/min, 12 l/min, and 20 l/min. The welding parameters used are presented in Table 4.

Table 4. Welding parameters used in the welding process

Current (A)	Voltage (V)	Advance Speed (cm/min)
110	18.1	50
110	18.1	50
110	18.1	50
Wire Feed Speed (m/min)	**Free Wire Length (mm)**	**Shielding Gas Flow Rate (l/min)**
6.4	15	5
6.4	15	12
6.4	15	20

Figure 3 presents a representative image of the welded test samples.

Figure 3. Sample image of welded parts

Figure 4 displays the tensile, notch impact, and microstructure test samples.

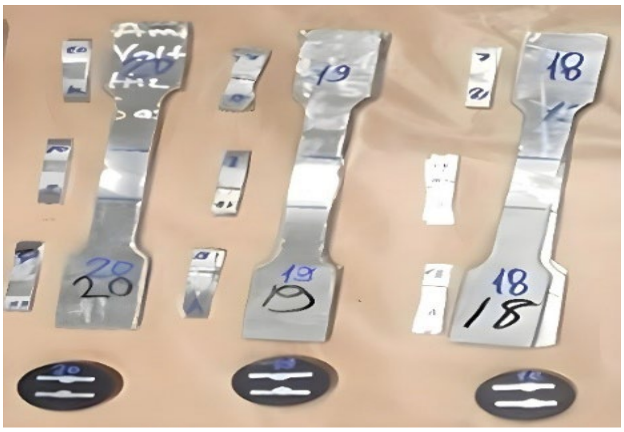

Figure 4. Tensile test, notch impact test and microstructure test samples **a)** 5 l/min (19), **b)** 12 l/min (18), **c)** 20 l/min (20)

2.2. Characterization of materials

The chemical analysis of the aluminum sheet and aluminum welding filler wire used in the experiments was conducted using a spectrometer (Spectrolab 5M). Additionally, tensile testing was performed with an Instron 300DX, notch impact testing with an Instron 300FT, and hardness testing with a Qness Q700M. The equipment used is shown in Figure 5.

Figure 5. Devices used for testing welded samples, spectrometer instrument (a), tensile tester (b), notched impact tester (c), hardness tester (d)

3. Results and Discussion

3.1. Tensile test results

Figures 6, 7, and 8 present the tensile testing results of the samples welded using different shielding gas flow rates. The tensile tests were conducted in accordance with the TS EN ISO 6892-1 standard.

The tensile strength and elongation values of samples welded at varying gas flow rates were measured using a tensile testing apparatus and presented in diagrams.

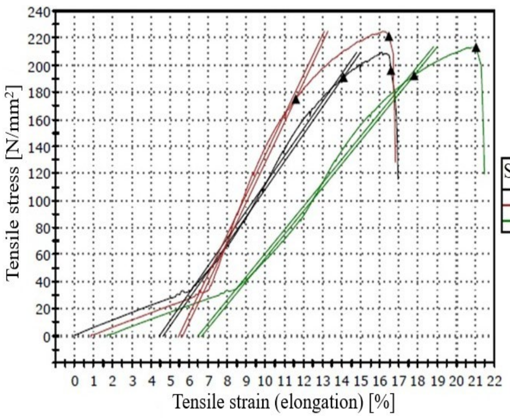

Figure 6. Graphical representation of tensile test samples which welded at a weld shield gas flow rate of 5 liters per minute

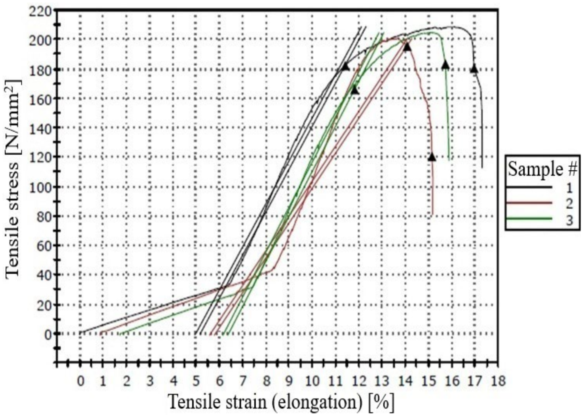

Figure 7. Graphical representation of tensile test samples which welded at a weld shield gas flow rate of 12 liters per minute

The results of the tensile tests are presented in Table 5. The tensile test results indicate that the sample welded with a shielding gas flow rate of 5 l/min has an average yield strength of 186 MPa, a tensile strength of 215 MPa, and an elongation of 10%. The sample welded at 12 l/min exhibits an average yield strength of 181 MPa, a tensile strength of 204 MPa, and 9% elongation. Meanwhile, the sample welded at a shielding gas flow rate of 20 l/min shows an average yield strength of 166 MPa, a tensile strength of 222 MPa, and an elongation of 10%.

Table 5. Table of tensile test results

Shielding Gas Flow Rate (l/min)	Yield Strength (MPa)	Tensile Strength (MPa)	Elongation (%)
5	186	215	10
12	181	204	9
20	166	222	10

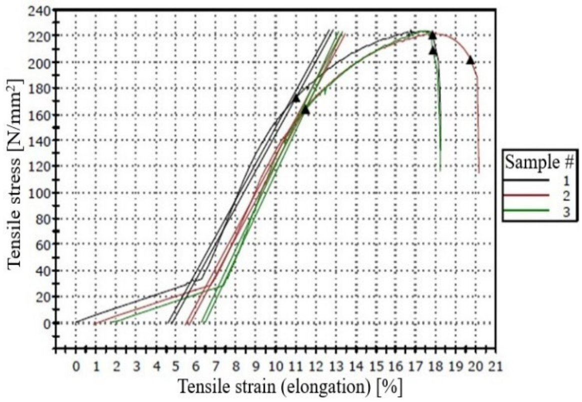

Figure 8. Graphical representation of tensile test samples which welded at a weld shield gas flow rate of 20 liters per minute.

According to the acceptance criterion specified in Table 2 of the EN 15614-2 Standard: Specification and Qualification of Welding Procedures for Metallic Materials–Arc Welding of Aluminium and Its Alloys, the tensile strength of the welded material must be at least 70% of the base material's tensile strength. The weldability results meet this requirement and are deemed satisfactory across all shielding gas flow rates.

Welded joints exhibit lower strength and elongation compared to the base metal region due to the heterogeneous microstructure that develops in different areas of the weld. The formation of a dendritic structure in the weld metal and grain coarsening in the heat-affected zone (HAZ) contribute to the reduction in tensile strength compared to the columnar grain structure of the base metal. Under tensile loading, stress becomes concentrated in the softened HAZ, ultimately causing the welded specimen to rupture. This is primarily attributed to the dissolution of hardening precipitates in the HAZ during the welding process [38].

3.2. Notch impact test results

To evaluate the energy absorbed by the welded samples during fracture under applied force, two specimens were taken from the base material, heat-affected zone (HAZ), and weld seam regions. A notch impact test was conducted, and the results are presented in Table 6. The test was performed using a V-notch in the welded samples, following the TS EN ISO 9016 standard.

Table 6. Notch impact test results

Shielding Gas Flow Rate (l/min)	Base Metal	HAZ	Welded Metal
Impact Toughness at 23°C (Joule)			
5	33	27	20
12	33	33	33
20	33	30	33
Impact Toughness at -20°C (Joule)			
Shielding Gas Flow Rate (l/min)	**Base Metal**	**HAZ**	**Welded Metal**
5	33	27	20
12	33	33	27
20	33	33	27

An analysis of the notch impact test results revealed a reduction in impact toughness in both the heat-affected zone (HAZ) and the weld metal region at all temperatures when using a shielding gas flow rate of 5 l/min. At a shielding gas flow rate of 12 l/min, impact toughness decreased in the weld metal region at -20°C. Similarly, at a shielding gas flow rate of 20 l/min, impact toughness declined in the HAZ at 23°C and in the weld metal region at -20°C. The decrease in notch impact strength with temperature is attributed to the material transitioning below the ductile-brittle transition temperature.

3.3. Hardness test results

The hardness of the welded samples was tested on the base metal, HAZ, and welded metal regions. Table 7 shows the results of the hardness test.

Table 7. Hardness test results

Shielding Gas Flow Rate (l/min)	Base Metal (HV)	HAZ (HV)	Welded Metal (HV)
5	63.5	63.5	63.5
12	72.4	52.1	65.5
20	71.6	67.1	58.5

An analysis of the hardness test results revealed only a slight difference in hardness between the base metal and the weld metal across all three samples. This is attributed to the use of an aluminum filler metal with properties similar to those of the base metal. However, the hardness in the heat-affected zone (HAZ) was lower than in both the weld metal and base metal. This reduction in hardness is primarily due to grain structure coarsening in the HAZ and the loss of strength resulting from heat input during welding.

The reduction in hardness and strength in welded joints can be attributed to precipitate phase transformations, grain coarsening, and changes in the dissolved element content. The microhardness values are expected to show a slight increase from the base metal toward the heat-affected zone (HAZ), while a slight decrease in hardness is anticipated from the HAZ toward the weld region.

An analysis of the hardness test results showed a slight difference in hardness between the base metal and weld metal regions in the samples welded at 12 l/min and 20 l/min. The heat-affected zone (HAZ) exhibited lower hardness compared to both the weld metal and base metal, primarily due to grain structure expansion and the loss of strength caused by heat input in this region. In contrast, the hardness values were consistent across all regions in the sample welded at 5 l/min.

The softening of the heat-affected zone (HAZ) in 6061-T6 aluminum alloy is influenced by various complex factors, including precipitate phase transitions, changes in elemental composition within the matrix, and variations in grain size. However, research on the microscopic mechanisms underlying HAZ softening in welded 6061-T6 aluminum alloy remains limited. Additionally, the extent to which these factors contribute to HAZ softening has not yet been fully established.

3.4. Macrostructure results

Figure 9 presents macrostructure images of all three samples. The weld cap and weld root areas formed at different shielding gas flow rates, as well as the welding defects that occurred, were assessed following the welding process.

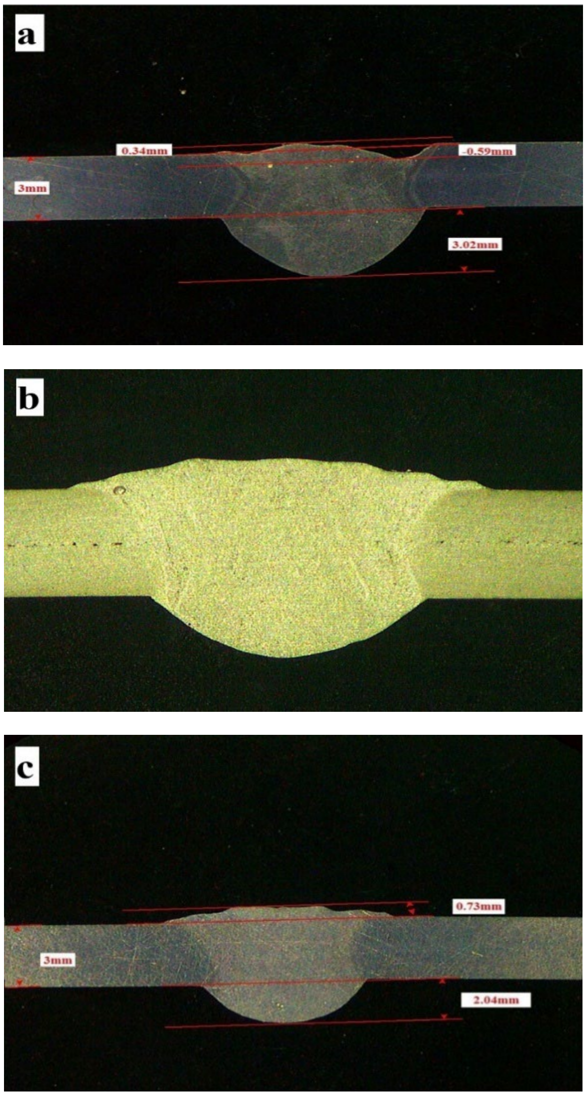

Figure 9. Macrographs of welded samples, a) 5 l/min shielding gas flow rate, b) 12 l/min shielding gas flow rate, c) 20 l/min shielding gas flow rate

As shown in the figure, the sidewall and root penetrations of all welded samples are within acceptable limits. The smallest weld cap size was recorded in the sample welded with a shielding gas flow rate of 5 l/min. Additionally, excessive root sagging was observed in this sample.

3.4. Microstructure results

Microstructure images were captured from multiple locations on the welded samples. To obtain microstructure images, the samples were sanded using 60–1200 grit sandpaper, polished with an alumina solution and polishing felt, and then etched with Keller's reagent (1 ml HF, 1.5 ml HCl, 2.5 ml HNO_3, 95 ml H_2O). After etching, the samples were examined under an optical microscope, and images were captured. Figures 10, 11, and 12 display the microstructure images of the base metal, heat-affected zone (HAZ), and weld metal regions of the welded samples at 100X magnification.

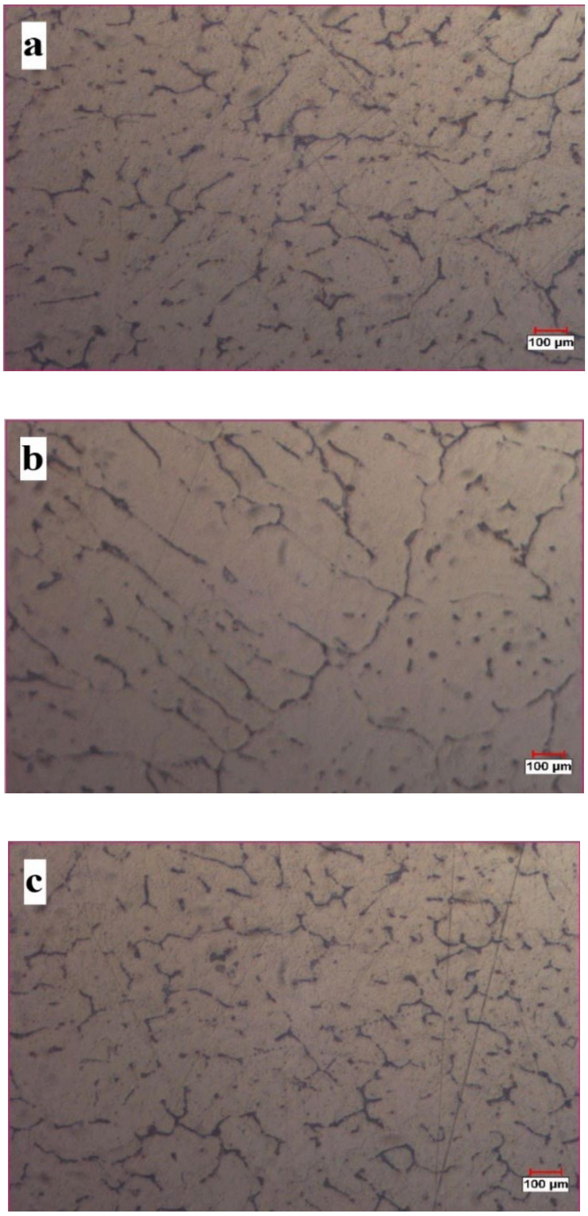

Figure 10. Micrograph images of the welded sample with 5 l/min protective gas flow rate, a) Base metal 100X, b) HAZ 100X, c) Welded metal 100X

After welding, distinct structural formations were observed in the base metal, heat-affected zone (HAZ), and weld metal regions. The microstructure of the welded samples can be broadly divided into three distinct regions: the weld region, the heat-affected zone (HAZ), and the base metal region. The weld region primarily consists of numerous dendritic grain structures along with equiaxed grains.

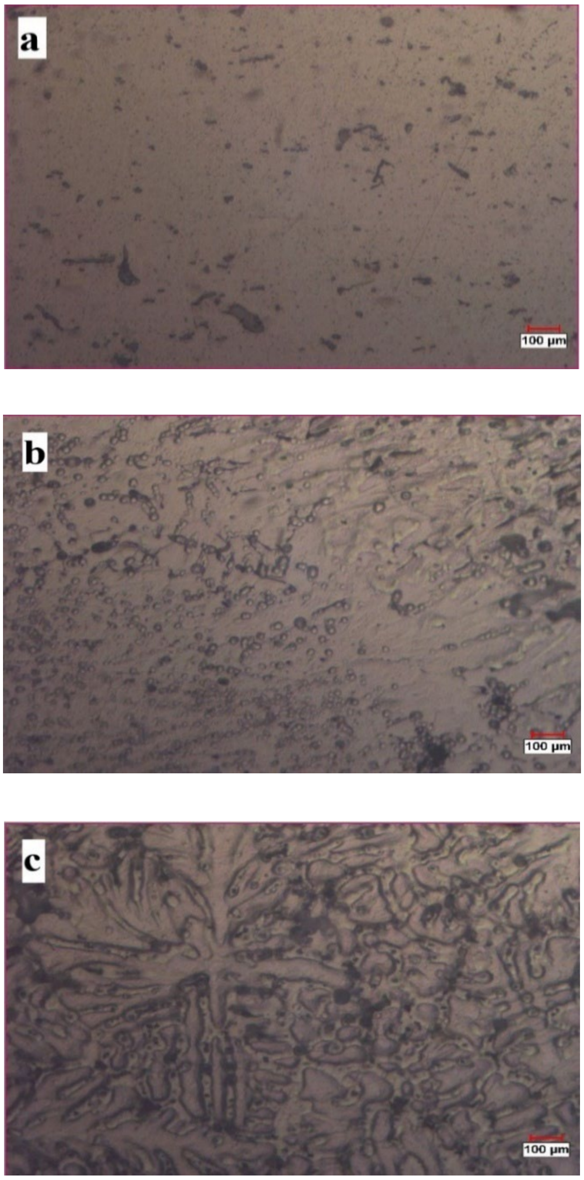

Figure 11. Micrograph images of the welded sample with 12 l/min protective gas flow rate, a) Base metal, 100X, b) HAZ 100X, c) Welded metal 100X

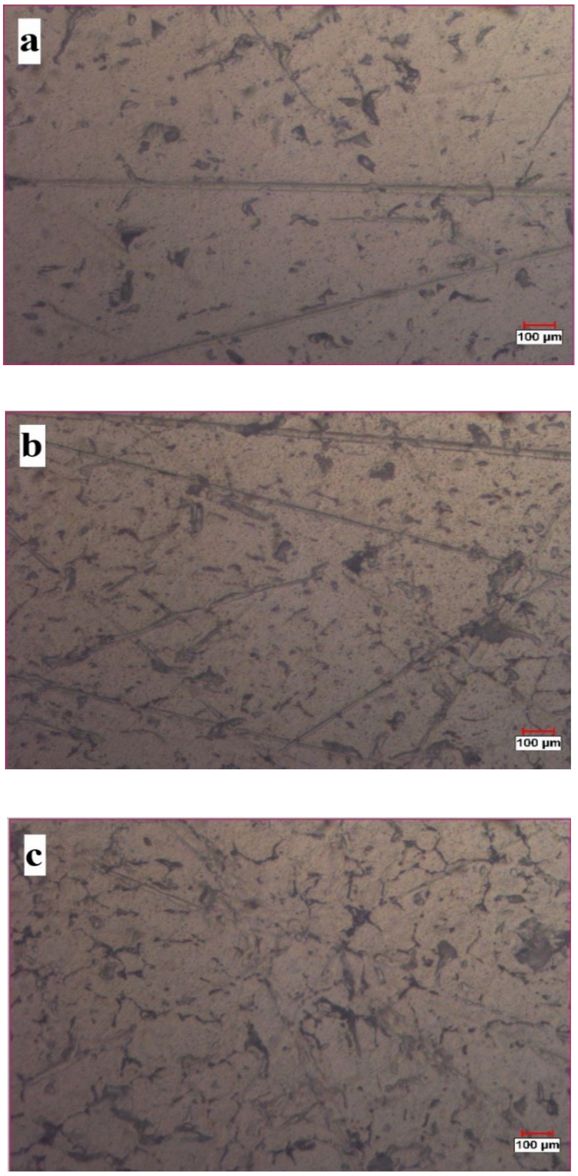

Figure 12. Micrograph images of the welded sample with 20 l/min protective gas flow rate, a) Base metal 100X, b) HAZ 100X, c) Welded metal 100X

A transition zone was present between the weld region and the heat-affected zone (HAZ). The microstructure of the HAZ was characterized by changes in grain morphology. The area of the HAZ closest to the weld experienced significant heating, leading to recrystallization within the rolled microstructure and the formation of large grains. This increase in grain size influences the mechanical properties of the welded joint, contributing to softening in the HAZ.

Additionally, the thermal cycling during welding alters the alloy's microstructure, further impacting the mechanical properties of the weld.

According to the literature, grain boundaries in the HAZ tend to grow as Mg_2Si structures due to the formation of silicon- and magnesium-rich precipitates. In contrast, the base metal region primarily consists of small equiaxed grains [39-44].

The welding thermal cycle affects the normal phase transformation of Al-Mg-Si alloys such as 6061-T6, and the β'' and β' phases formed during the Al-Mg-Si precipitation stages have a very important effect on the strength of Al-Mg-Si alloys. Their amount, size and distribution directly affect the mechanical properties of these alloys [45-49].

The complex welding thermal cycle in these alloys, along with the resulting variations in dissolved element content across different regions of the joint, leads to microstructural transformations. These changes make it challenging to fully understand the underlying causes of the deterioration in the joint's mechanical properties [50-52].

During the welding process of Al-Mg-Si alloys, the arc melts both the welding wire and a portion of the base metal, forming a molten pool. The temperature of this molten pool exceeds the dissolution temperature of the β′ and β″ phases, causing the nanoscale β′ and β″ phases in the base metal to completely dissolve. During the subsequent cooling process, these phases precipitate as large β-Mg_2Si phases. Additionally, some of the Mg element in the base metal is burned off during welding, contributing to the softening of the weld zone. The combined effects of β-Mg_2Si phase precipitation and Mg element loss lead to significant weld zone softening. Since the β-Mg_2Si phase is incompatible with the α(Al) matrix and provides minimal strengthening, it further exacerbates softening in the weld zone. The transformation behavior of the primary strengthening phase (β″) in the base metal during the welding thermal cycle is the key factor responsible for this softening [53, 54].

Due to its low heat input characteristics and the absence of surface porosity and other defects on the weld surface, the TPSi welding method is suitable for use [55].

4. Conclusion

The data obtained as a result of the study are shown below.

- The welded samples exhibited lower tensile and yield strengths compared to the base metal. The tensile strength varied depending on the shielding gas flow rate. The highest tensile strength was observed in samples welded at a shielding gas flow rate of 20 l/min, while the highest yield strength was recorded in samples welded at a flow rate of 5 l/min.

- An analysis of the notch impact test results revealed that the impact toughness of the heat-affected zone (HAZ) and weld metal regions decreased at all temperatures when a shielding gas flow rate of 5 l/min was used. It was found that low shielding gas flow rates directly influence notch impact energy.

- Vickers hardness values were determined for the base metal, HAZ, and welded metal regions in each shielding gas flow sample and found to be comparable.

- An examination of the macrostructure images revealed that the desired weld filler metal height in the cap was not achieved in the sample welded with a shielding gas flow rate of 5 L/min.

- An analysis of the microstructure samples revealed that the images obtained from the base metal, heat-affected zone (HAZ), and weld metal regions in all three samples were highly similar.

In conclusion, 6061-T6 aluminum sheets, which are widely used in the industry, were successfully welded using the MIG welding process (TPS/i) with optimal shielding gas flow rate parameters.

Article Information Form

Authors' Contribution

Erman Ferik wrote the paper, reviewed the content critically, and conducted a literature review.
Sedat Dağlaraştı handled conception, data collecting, and material assistance.
Faruk Varol handled design, data collecting, and technical support.

The Declaration of Conflict of Interest/ Common Interest

No conflict of interest or common interest has been declared by authors.

Artificial Intelligence Statement

No artificial intelligence tools were used while writing this article.

References

[1] E. L. Persson, Aluminum Alloys: Preparation, Properties, and Applications, New York: Nova Science Publishers Inc, 2011.

[2] G. E. Toten, D. S. Mackenzie (eds.), Handbook of Aluminum: Volume 1: Physical Metallurgy and Processes, New York: Marcel Dekker Inc, 2003.

[3] K. Anderson, J. Weritz, J. G. Kaufman (eds.), ASM Handbook Volume 2A - Aluminum Science and Technology, Ohio: ASM International, 2018.

[4] Z. Fang, J. Cao, Y. Guan, Corrosion Control Technologies for Aluminum Alloy Vessel, Singapore: Springer, 2020.

[5] H. Abramovich, Advanced Aerospace Materials: Aluminum-Based and Composite Structures, 2nd ed. Berlin: Walter de Gruyter GmbH, 2023.

[6] H. Liu, J. Li, Z. Ma, B. Ma, S. Feng, "Study on mechanical properties and microstructure analysis of welded joints of 7A05 aluminum alloy by laser-MIG hybrid welding," In 2nd International Conference on Electronic & Mechanical Engineering and Information Technology, France: Atlantis Press, 2012, pp. 1465-1470.

[7] G. E. Totten, M. Tiryakioglu, O. Kessler (eds.), Encyclopedia of Aluminum and Its Alloys, Boca Raton: CRC Press, 2018.

[8] V. S. Zolotorevsky, N. A. Belov, M. V. Glazoff, Casting Aluminum Alloys, Oxford: Elsevier Ltd, 2007.

[9] J. R. Davis, Aluminum and Aluminum Alloys, Ohio: ASM International, 1999.

[10] L. F. Mondolfo, Aluminum Alloys: Structure and Properties, London: Butterworth-Heinemann, 1976.

[11] The Aluminum Association, Aluminum Design Manual, Specifications & Guidelines for Aluminum Structures, 8th ed. Washington: The Aluminum Association, Inc, 2005.

[12] G. E. Totten, D. S. MacKenzie, Handbook of Aluminum: Volume 2: Alloy Production and Materials Manufacturing, New York: Marcel Dekker Inc, 2003.

[13] J. G. Kaufman, Introduction to Aluminum Alloys and Tempers, Ohio: ASM International, 2000.

[14] J. R., Kissell, R. L. Ferry, Aluminum Structures: A Guide to Their Specifications and Design, 2nd ed. New York: John Wiley & Sons, 2002.

[15] H. J. McQueen, S. Spigarelli, M. Kassner, E. Evangelista, Hot Deformation and Processing of Aluminum Alloys, Boca Raton: CRC Press, 2016.

[16] D. Luo, Y. Xiao, L. Hardwick, R. Snell, M. Way, X. S. Morell, F. Livera, N. Ludford, C. Panwisawas, H. Dong, R. Goodall, "High entropy alloys as filler metals for joining," Entropy, vol. 23, no. 1, pp. 78-101, 2021.

[17] S. Anık, Kaynak Tekniği El Kitabı: Yöntemler ve Donanımlar, İstanbul: Gedik Eğitim Vakfı, 1991.

[18] D. H. Phillips, Welding Engineering An Introduction, 2nd ed. New Jersey: John Wiley & Sons, Inc., 2023.

[19] N. Kahraman, B. Gülenç, Modern Kaynak Teknolojisi ve Kaynak İşlerinde İş Sağlığı ve Güvenliği, Genişletilmiş 4. Baskı. Epa-Mat Basım Yayın Ltd, Şti: Ankara, 2020.

[20] G. Çam, Kaynak Bilimi ve Teknolojisi, Ankara: Nobel Akademik Yayıncılık, 2020.

[21] A. Çelik, Kaynak Teknolojileri, Ankara: Nobel Akademik Yayıncılık, 2020.

[22] S. E. Hughes, A Quick Guide to Welding and Weld Inspection, Cambridge: Woodhead Publishing, 2009.

[23] R. L. O'Brien, Welding Handbook. Volume 2: Welding Processes: Part 1, 9th ed. Miami: American Welding Society, 2004.

[24] K. Weman, G. Lindén, (eds.), MIG Welding Guide, Cambridge: Woodhead Publishing, 2006.

[25] T. Anderson, Welding Aluminum: Questions and Answers: A Practical Guide for Troubleshooting Aluminum Welding-related Problems, 2nd ed. Miami: American Welding Society, 2010.

[26] Fronius International Gmbh. (2025.05.20) TransSynergic 4000/5000, TransPuls Synergic 2700, TransPuls Synergic 3200/4000/5000, TIME 5000 Digital, CMT 4000 Advanced Kullanım Kılavuzu [Online]. Available: https://www.alganmetal.com.tr/images/gallery_files/74814ts_tps_kullanim_kilavuzu_yeni.pdf

[27] K. R. Madavi, B. F. Jogi, G. S. Lohar, "Metal Inert Gas (MIG) Welding Process: A Study of Effect of Welding Parameters," Materials Today: Proceedings, vol 51, pp. 690-698, 2022.

[28] G. M. Evans, N. Bailey, Metallurgy of Basic Weld Metal, Cambridge: Woodhead Publishing Limited, 1997.

[29] K. Badwal, P. Khanna, "Investigation of effect of shielding gases on angular distortion and bead profile parameters of MIG welded stainless steel 409L plates," Materials Today: Proceedings, vol 56, pp. 645-649, 2022.

[30] Z. H. Rao, J. Hu, S. M. Liao, H. L. Tsai, "Study the shielding gas effect on the metal transfer and weld pool dynamics in GMAW," In Heat Transfer Summer Conference, California, USA, vol. 43581, 2009, pp. 675-684.

[31] C. Cai, S. He, H. Chen, W. Zhang, "The influences of Ar-He shielding gas mixture on welding characteristics of fiber laser-MIG hybrid welding of aluminum alloy," Optics & Laser Technology, vol. 113, pp. 37-45, 2019.

[32] S. W. Campbell, A. M. Galloway, G. M. Ramsey, N. A. McPherson, "A potential solution to GMAW gas flow optimisation," In Trends in Welding Research 2012: Proceedings of the 9th International Conference, Chicago, USA, pp. 453-460, 2012.

[33] G. D. Uttrachi, "GMAW shielding gas flow control systems," Welding Journal, vol. 86, no. 4, pp. 22-23, 2007.

[34] S. W. Campbell, A. M. Galloway, N. A. McPherson, "Techno-economic evaluation of reducing shielding gas consumption in GMAW whilst maintaining weld quality," The International Journal of Advanced Manufacturing Technology, vol. 63, pp. 975-985, 2012.

[35] W. Lucas, S. Westgate, "Welding and Soldering," in Electrical Engineer's Reference Book, M. A. Laughton, D. J. Warne Eds. Oxford: Elsevier Science, pp. 246-298, 2003.

[36] C. Rajendran, T. Sonar, M. Ivanov, C. Sandeep, C. Shanthi, N. K. Gurajala, K. Balachandar, J. Xu, "Enhancing tensile properties of pulsed CMT–MIG welded high strength AA2014-T6 alloy joints: effect of post weld heat treatment," International Journal of Lightweight Materials and Manufacture, vol. 7, no. 2, pp. 344-352, 2024.

[37] Z. Ye, H. Zhu, S. Wang, W. Wang, J. Yang, J. Huang, "Fabricate high-strength 7075 aluminum alloy joint through double pulse MIG welding process," Journal of Manufacturing Processes, vol. 125, pp. 512-522, 2024.

[38] V. Singh, Q. Murtaza, M. S. Niranjan, “Microstructure and mechanical properties of CMT welded AA6063-T6/B4C/ES metal matrix composite using ER5356 filler wire,” Materials Today: Proceedings, 2024.

[39] S. T. Selvamani, “Microstructure and stress corrosion behaviour of CMT welded AA6061 T-6 aluminium alloy joints,” Journal of Materials Research and Technology, vol. 15, pp. 315-326, 2021.

[40] Z. Shen, R. H. Wagoner, W. A. T. Clark, “Dislocation and grain boundary interactions in metals,” Acta Metallurgica, vol. 36, no. 12, pp. 3231-3242, 1988.

[41] M. P. Anderson, D. J. Srolovitz, G. S. Grest, P. S. Sahni, “Computer simulation of grain growth—I. kinetics,” Acta Metallurgica, vol. 32, no. 5, pp. 783-791, 1984.

[42] S. Yang, X. Yang, X. Lu, M. V. Li, H. Zuo, Y. Wang, “Strength calculation and microstructure characterization of haz softening area in 6082-T6 aluminum alloy CMT welded joints,” Materials Today Communications, vol. 37, 107077, 2023.

[43] M. Zhu, S. Yang, Y. Bai, C. Fan, “Uneven hardness mechanism and related fracture characteristics in laser-MIG hybrid welded Al–Mg–Si alloy butt,” Journal of Laser Applications, vol. 33, no. 4, pp. 42-54, 2021.

[44] M. A. Van Huis, J. H. Chen, H. W. Zandbergen, M. H. F. Sluiter, “Phase stability and structural relations of nanometer-sized, matrix-embedded precipitate phases in Al–Mg–Si alloys in the late stages of evolution,” Acta Materialia, vol. 54, no. 11, pp. 2945-2955, 2006.

[45] J. H. Chen, E. Costan, M. A. Van Huis, Q. Xu, H. W. Zandbergen, “Atomic pillar-based nanoprecipitates strengthen AlMgSi alloys,” Science, vol. 312, no. 5772, pp. 416-419, 2006.

[46] C. D. Marioara, H. Nordmark, S. J. Andersen, R. Holmestad, “Post-β″ phases and their influence on microstructure and hardness in 6xxx Al-Mg-Si alloys,” Journal of Materials Science, vol. 41, pp. 471-478, 2006.

[47] H. Liu, S. Yang, C. Xie, Q. Zhang, Y. Cao, “Microstructure characterization and mechanism of fatigue crack initiation near pores for 6005A CMT welded joint,” Materials Science and Engineering: A, vol. 707, pp. 22-29, 2017.

[48] Z. Yang, I. Erdle, C. Liu, J. Banhart, “Clustering and precipitation in Al-Mg-Si alloys during linear heating,” Journal of Materials Science & Technology, vol. 120, pp. 78-88, 2022.

[49] X. Xu, W. Zhu, X. Guo, C. Liang, Y. Deng, “Effect of ageing treatment process on the microstructure development and mechanical properties of 6082 Al alloy,” Journal of Alloys and Compounds, vol. 935, no. 1, 167892, 2023.

[50] S. Yang, Y. Wang, X. Yang, X. Lu, M. V. Li, X. Zhu, “Effect of softening of 6082-T6 aluminum alloy CMT welded joints on mechanical properties and fracture behavior,” Journal of Manufacturing Processes, vol. 124, pp. 1567-1582, 2024.

[51] I. Guzmán, E. Granda, B. Vargas, C. Cruz, Y. Avila, J. Acevedo, “Tensile and fracture behavior in 6061-T6 and 6061-T4 aluminum alloys welded by pulsed metal transfer GMAW,” The International Journal of Advanced Manufacturing Technology, vol. 103, pp. 2553-2562, 2019.

[52] Z. Yang, I. Erdle, C. Liu, J. Banhart, “Clustering and precipitation in Al-Mg-Si alloys during linear heating,” Journal of Materials Science & Technology, vol. 120, pp. 78-88, 2022.

[53] Q. T. Wang, X. N. Wang, X. M. Chen, P. C. Huan, Q. P. Dong, Q. Y. Zhang, H. Nagaumi, “Interactive effects of porosity and microstructure on strength of 6063 aluminum alloy CMT MIX+ Synchropulse welded joint,” Transactions of Nonferrous Metals Society of China, vol 32, no. 3, pp. 801-811, 2022.

[54] J. A. Vargas, J. E. Torres, J. A. Pacheco, R. J. Hernandez, “Analysis of heat input effect on the mechanical properties of Al-6061-T6 alloy weld joints,” Materials & Design (1980-2015), vol. 52, pp. 556-564, 2013.

[55] M. V. Kumar, V. Balasubramanian, S. Rajakumar, S. K. Albert, “Stress corrosion cracking behaviour of gas tungsten arc welded super austenitic stainless steel joints,” Defence Technology, vol. 11, no. 3, pp. 282-291, 2015.